Quantum Chemistry Based Statistical Mechanical Model of Hydrogen Desorption from Si(100)-2 × 1, Ge(100)-2 × 1, and SiGe Alloy Surfaces

Collin Mui and Stacey F. Bent

Department of Chemical Engineering, Stanford University, Stanford, California 94305

Charles B. Musgrave*

Departments of Chemical Engineering and Materials Science and Engineering, Stanford University, Stanford, California 94305

Received: December 19, 2003; In Final Form: August 27, 2004

A model for temperature programmed desorption (TPD) of hydrogen from the Si(100)-2 × 1, Ge(100)-2 × 1, and SiGe alloy surfaces is presented. In the model, density functional theory is used to calculate the activation barriers of hydrogen desorption, and statistical mechanics is applied to determine the distribution of hydride species on the Si(100)-2 × 1, Ge(100)-2 × 1, and SiGe alloy surfaces using the DFT results. Hydrogen desorption via both the prepairing mechanism and the interdimer mechanisms is considered. The overall rates of hydrogen desorption from the surfaces are determined by the statistical model, and TPD spectra are simulated from the overall desorption rates. We find that, although the TPD spectra simulated according to the prepairing mechanism are consistent with the near-first-order kinetics observed experimentally on the Si(100)-2 × 1 and Ge(100)-2 × 1 surfaces, hydrogen desorption via interdimer mechanisms results in peak temperatures more consistent with experiments. We also consider two kinetic models which combine the contributions from both mechanisms and find better agreement with experiments in terms of both desorption peak temperatures and reaction orders. Finally, we have modeled hydrogen desorption from SiGe alloy surfaces.

I. Introduction

Silicon−germanium (SiGe) alloy thin films have attracted significant interest in recent years due to the applications of SiGe in complementary metal-oxide-semiconductor (CMOS) technology, telecommunications, optoelectronics, and quantum effect devices.[1−5] Deposition of SiGe alloys is commonly achieved by chemical vapor deposition (CVD) or gas-source molecular beam epitaxy (GSMBE) with Si and Ge hydrides as gas-phase precursors.[6−8] Elementary surface processes during alloy deposition include adsorption of precursors, surface reaction, and desorption of byproducts. However, the detailed mechanisms and the kinetic parameters of the surface reactions, especially those on alloy surfaces, are mostly unknown.

Since the initial observation of first-order desorption of hydrogen from the Si(100)-2× 1 surface,[9] there has been intense interest in the mechanism and associated kinetics of hydrogen desorption from the Si(100)-2 × 1 surface.[10,11] Several mechanisms have been proposed, including the prepairing,[9,12−14] dihydride,[15,16] and interdimer mechanisms[17−19] and desorption via an excited electronic state.[20] The prepairing mechanism involves only one surface dimer, on which the two hydrogen atoms pair up and recombine to form H_2, which desorbs directly from the dimer, as shown in Scheme 1. The prepairing mechanism is a natural consequence of the weak π interaction between the two atoms of a bare dimer, which results in a thermodynamic driving force for surface hydrogen atoms to pair up and form the monohydride phase. When combined with the lattice gas model, the prepairing mechanism is able to explain the first-order kinetics of hydrogen desorption from the Si(100)-2 × 1 and Ge(100)-2 × 1 surfaces.[12,13,21,22] However, calculations employing smaller cluster models for the surface tend to overestimate the activation barrier for hydrogen desorption from the Si(100)-2 × 1 surface.[14,15,23]

SCHEME 1

Interdimer mechanisms, suggested by recent scanning tunneling microscopy (STM) and second harmonic generation (SHG) studies, involve recombinative desorption from two Si−H bonds on two adjacent dimers along a dimer row.[17−19] Three interdimer mechanisms for hydrogen desorption from the Si(100)-2 × 1 surface have been proposed based on STM and SHG experiments, namely the 2H, 3H, and 4H mechanisms.[17] In the 2H desorption mechanism shown in Scheme 2, hydrogen

SCHEME 2

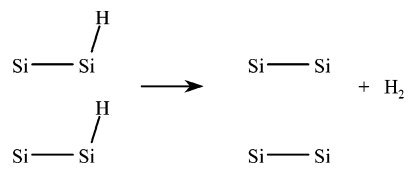

* Corresponding author: chasm@stanford.edu.

10.1021/jp0379493 CCC: $27.50
Published on Web 11/03/2004

atoms recombinatively desorb from two adjacent singly occupied dimers. The 3H mechanism in Scheme 3 involves desorption

SCHEME 3

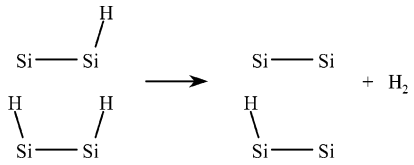

from adjacent singly and doubly occupied dimers. Finally, the 4H desorption mechanism in Scheme 4 involves desorption from adjacent doubly occupied dimers.

SCHEME 4

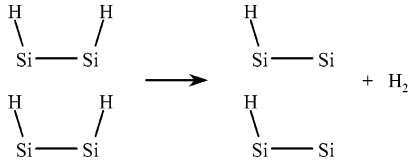

Although extensive theoretical and experimental studies have been performed on the Si(100)-2 × 1 surface, there are relatively fewer studies on SiGe alloy surfaces. In particular, the mechanism of hydrogen desorption from SiGe alloy surfaces and the effect of Ge alloying atoms on the kinetics of hydrogen desorption are not well understood.[24−31] Therefore, we use DFT to study the kinetics and mechanisms of hydrogen desorption from SiGe alloy surfaces. We will focus on the prepairing and interdimer mechanisms in this work because these mechanisms are the most well accepted mechanisms and are fundamentally different, in that they involve a different number of surface sites. Consequently, the effect of surface Ge on hydrogen desorption from SiGe alloy surfaces via the prepairing and interdimer mechanisms are expected to be different. We have calculated the activation barriers of hydrogen desorption via both mechanisms using cluster models and report the details of the DFT calculations in a separate paper.[32]

Here, we present a model based on the statistical distribution of hydride species determined using DFT energies to explain TPD experiments on the Si(100)-2 × 1 and Ge(100)-2 × 1 surfaces. The model uses the calculated kinetic parameters from both the prepairing and interdimer mechanisms to simulate desorption rates and TPD spectra of hydrogen desorption from the Si(100)-2 × 1 and Ge(100)-2 × 1 surfaces. We find that the calculated rates of hydrogen desorption via the prepairing mechanism are slower than the interdimer desorption rates. However, whereas hydrogen desorption via the prepairing mechanism exhibits near-first-order behavior with an apparent reaction order that ranges from 1.17 to 1.71, the apparent reaction order for hydrogen desorption via the interdimer mechanisms ranges from 2.01 to 2.46. We will discuss the general features of the simulated TPD spectra and compare them with experiments on the Si(100)-2 × 1 and Ge(100)-2 × 1 surfaces. In addition, a model for hydrogen desorption from SiGe alloy surfaces will be presented. Finally, we discuss the limitations of our models.

II. Theoretical Approach

A. Quantum Chemistry Calculations. The quantum chemistry calculations are based on DFT[33,34] employing the B3LYP three-parameter hybrid exchange-correlation functional[35] as implemented in the Gaussian 98 computational chemistry software package.[36] Cluster models consisting of one to four dimers are used to simulate hydrogen desorption via prepairing and interdimer mechanisms. For example, the Si_9H_{12} cluster is the smallest cluster we use to model one dimer on the Si(100)-2 × 1 surface. On the other hand, the $Ge_8Si_{19}H_{24}$ cluster consists of four Ge−Ge homodimers on the surface and is the largest cluster we use to model the Ge(100)-2 × 1 surface. The electronic structure is expanded in a mixed Gaussian basis set, which uses the 6-311++G(d,p) and 6-31G(d) basis sets for the active and subsurface atoms, respectively. We have determined the structures and energies of the minima and transition states for hydrogen desorption by both constrained and unconstrained geometry optimization procedures. The energies reported are zero-point-corrected unless otherwise stated. All details of the quantum chemistry calculations, including the construction of the cluster models, the mixed basis set scheme, and procedures of constrained geometry optimization, are discussed in a separate paper.[32]

B. Physical and Surface Chemistry Model of TPD. Our approach for the simulation of TPD spectra is based on the combined physical and surface chemistry model of Russell and Ekerdt.[37] During a TPD experiment, the sample is heated and the adsorbed species desorb from the surface, resulting in a transient pressure rise recorded by a mass spectrometer. The temperature at which desorption occurs depends on how strongly the adsorbate is bonded onto the surface. Therefore, the TPD model consists of a physical description of the transient pressure rise resulting from species desorption from the surface and a surface chemical description of the desorption rate of the species at different temperatures.

The relationship between the desorption rate of a species from a surface and the transient pressure rise is generally complex, since the signal measured by the mass spectrometer depends on the characteristics of the vacuum system, the sensitivity of the mass spectrometer, and the desorption rate of the species. However, the signal response can be modeled by eq 1, which relates the pressure and the desorption rate as a function of time[37]

$$p(t) = p_{eq} + a\int_0^t \frac{d\theta(t')}{dt'} \exp\left[\frac{-(t-t')}{\tau}\right] dt' \qquad (1)$$

In eq 1, p_{eq}, τ, and a are the base pressure, the characteristic pumping speed of the vacuum system, and the sensitivity factor of the mass spectrometer, respectively. $[d\theta(t')]/[dt']$ is the total desorption rate of the surface species of interest. Whereas most of the parameters in the physical model are characteristic of the experimental system, adsorbate−surface chemical interactions govern the desorption rate $[d\theta(t')]/[dt']$ and are thus an essential element of the model that determines the shape of the TPD spectra. In general, the desorption rate is a function of the coverage of all of the surface species, as well as the surface temperature. The exact functional form of the desorption rate can be deduced from a set of differential equations that describes the surface chemistry of the desorption process (2)

$$\frac{d\theta}{dt} = f\left(\theta, \frac{d\theta}{dt}, T\right) \qquad (2)$$

C. Prepairing of Hydrogen Atoms and Surface Hydride Distribution. The premise of the prepairing mechanism is that hydrogen atoms diffuse on the surface and pair up on the dimers before desorption. A lattice gas model to describe the distribution of different hydride species for hydrogen desorption via the prepairing mechanism was introduced by D'Evelyn et al.[22] In

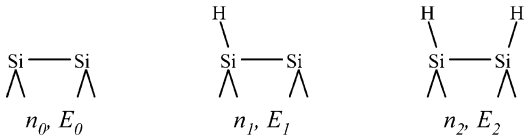

Figure 1. Hydride species on the Si(100)-2 × 1 surface for the prepairing mechanism.

this model, the partition function, Z, given by eq 3, includes contributions from unoccupied, singly occupied and doubly occupied dimers, denoted by n_0, n_1, and n_2, respectively and shown in Figure 1. The distribution of the hydride species depends on the relative energies of the species E_0, E_1, and E_2, as well as the temperature T

$$Z = \frac{N!}{n_0!\,n_1!\,n_2!}\,2^{n_1}\exp\left[-\frac{n_0E_0 + n_1E_1 + n_2E_2}{RT}\right] \qquad (3)$$

An analytical solution exists if the partition function is minimized with constraints determined by the hydride species balance. The resulting rate of hydrogen desorption is given by a first order expression (4) in which the coverage of doubly occupied dimers θ_2 is written as a function of the total coverage θ, the π-bond strength ϵ, and $\beta = 1/RT$. The rate constant for hydrogen desorption, k, consists of a preexponential factor ν and an activation barrier E_A

$$\frac{d\theta}{dt} = -k\theta_2 = -\nu\exp\left(-\frac{E_A}{RT(t)}\right)\left[\theta - \frac{2\theta(1-\theta)}{1+\sqrt{4\theta(1-\theta)(e^{\beta\epsilon}-1)}}\right] \qquad (4)$$

To simulate a TPD spectrum for hydrogen desorption via the prepairing mechanism, the differential equation (4) describing the desorption process is solved with DFT-calculated rate constants. The TPD spectrum is then simulated from the convolution of the desorption rate and the pumping speed described by the physical model (1).

D. Hydride Species Distribution for Interdimer Mechanisms. Since interdimer mechanisms involve two adjacent surface dimers, the distribution of hydride species on the surface is more complicated. Specifically, all of the possible hydride species on two adjacent surface dimers must be included. Similar to the prepairing mechanism, we assume an equilibrium distribution of the hydride species on the surface. Also, we extend the statistical approach of D'Evelyn et al. to include contributions from the seven nondegenerate configurations (Figure 2) for hydride species on two adjacent dimers and the partition function for this system is given in eq 5 where i denotes the hydride species

$$Z = \frac{N!2(n_{adj}+n_{alt}+n_{mono})\,4(n_{21}+n_{10})}{n_{22}!\,n_{21}!\,n_{adj}!\,n_{alt}!\,n_{mono}!\,n_{10}!\,n_{00}!}\exp\left(-\beta\sum_i n_iE_i\right) \qquad (5)$$

To determine the equilibrium coverages of all the interdimer hydride species on a dimerized group IV semiconductor surface at a given temperature, the partition function is minimized with constraints determined by a hydride species balance. Two species balance equations, (6) and (7), can be written. The first concerns the surface hydrogen coverage $4M$ and the second gives the total number of surface sites N. The minimization procedure results in a set of equations, each describing the coverage of one hydride species (8), where λ_M and λ_N are the

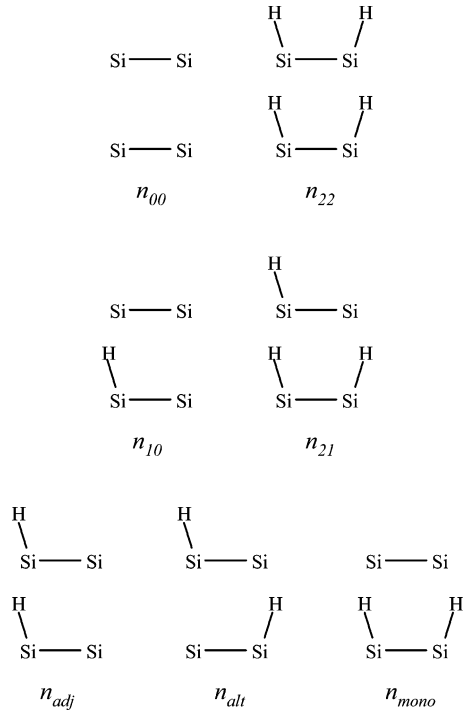

Figure 2. Hydride species on the Si(100)-2 × 1 surface for the interdimer mechanisms.

Lagrange multipliers for the two constraints (6) and (7), respectively

$$4M = 4n_{22} + 3n_{21} + 2(n_{adj} + n_{alt} + n_{mono}) + n_{10} \qquad (6)$$

$$N = n_{22} + n_{21} + n_{adj} + n_{alt} + n_{mono} + n_{10} + n_{00} \qquad (7)$$

$$\begin{aligned} n_{22} &= e^{-\beta E_{22}+4\lambda_M+\lambda_N} \\ n_{21} &= 4e^{-\beta E_{21}+3\lambda_M+\lambda_N} \\ n_{adj} &= 2e^{-\beta E_{adj}+2\lambda_M+\lambda_N} \\ n_{alt} &= 2e^{-\beta E_{alt}+2\lambda_M+\lambda_N} \\ n_{mono} &= 2e^{-\beta E_{mono}+2\lambda_M+\lambda_N} \\ n_{10} &= 4e^{-\beta E_{10}+\lambda_M+\lambda_N} \\ n_{00} &= e^{-\beta E_{00}+\lambda_N} \end{aligned} \qquad (8)$$

The total rate of hydrogen desorption from interdimer mechanisms consists of contributions from the 2H, 3H, and 4H mechanisms. Hence the rate expression (9) contains only terms involving n_{22}, n_{21}, and n_{adj}, and the rate constants consist of kinetic parameters of the three pathways (10). To simulate a TPD spectrum, the set of differential-algebraic equations, which consists of the rate expression for hydrogen desorption (9) and (10), the distribution of all hydride species on the semiconductor surface (8), and the species balance constraints, given by eqs 6 and 7, are solved numerically for a linear temperature ramp

$$\frac{d\theta}{dt} = -\frac{k_{4H}}{2}n_{22} - \frac{k_{3H}}{2}n_{21} - \frac{k_{2H}}{2}n_{adj} \qquad (9)$$

$$\begin{aligned} k_{4H} &= \nu_{4H}\exp\left[-\frac{E_{4H}}{RT(t)}\right] \\ k_{3H} &= \nu_{3H}\exp\left[-\frac{E_{3H}}{RT(t)}\right] \\ k_{2H} &= \nu_{2H}\exp\left[-\frac{E_{2H}}{RT(t)}\right] \end{aligned} \qquad (10)$$

At each temperature step, the partition function is minimized with species balance constraints to determine the distribution of hydride species, and the total rate of hydrogen desorption is calculated. As the temperature increases, the desorption rate increases and the total hydrogen coverage decreases. Finally, a TPD spectrum is simulated from the convolution of the desorption rate and pumping speed described by the physical model of TPD in eq 1.

E. Prepairing of Hydrogen Atoms on SiGe Alloy Surfaces. The hydride species distribution on SiGe alloy surfaces can be derived by extending the prepairing model on the Si(100)-2 × 1 surface. In particular, Vizoso et al. developed a statistical model to include the contributions from different SiGe dimers on SiGe alloy surfaces.[38] In the model, the partition function for the hydride species is given by eq 11, in which different dimers are denoted by superscripts. For example, n_1^{Ge-Ge} represents the number of singly occupied Ge−Ge dimers. There are two possible singly occupied Ge−Si heterodimers, denoted by n_1^{Si-GeH} and n_1^{SiH-Ge}. The distribution of the hydride species depends on the relative energies of the species E_i^j, where i is the occupation and j is the dimer species, as well as the temperature T

$$Z = \frac{N^{Si-Si}!}{n_0^{Si-Si}!\,n_1^{Si-Si}!\,n_2^{Si-Si}!} \times \frac{N^{Si-Ge}!}{n_0^{Si-Ge}!\,n_1^{Si-GeH}!\,n_1^{Ge-SiH}!\,n_2^{Si-Ge}!} \frac{N^{Ge-Ge}!}{n_0^{Ge-Ge}!\,n_1^{Ge-Ge}!\,n_2^{Ge-Ge}!} \times 2(n_1^{Si-Si} + n_1^{Ge-Ge}) \exp\left[-\frac{1}{RT}\sum_{i=0,1,2;j} n_i^j E_i^j\right] \quad (11)$$

We apply the method of Vizoso et al. to determine the equilibrium coverages of all of the hydride species on a SiGe alloy surface at a given temperature, which involves minimizing the partition function with constraints given by hydride species balance.[38] Using the hydride species distribution, a rate expression can be derived for hydrogen desorption from SiGe alloy surfaces, which only contains terms involving doubly occupied dimers according to the prepairing mechanism (12). A TPD spectrum for hydrogen desorption from a SiGe alloy surface via the prepairing mechanism can then be simulated using a procedure similar to that for the prepairing and interdimer mechanisms

$$\frac{d\theta}{dt} = -k_{Si-Si}n_2^{Si-Si} - (k_{Ge-Si^*} + k_{Ge^*-Si})n_2^{Si-Ge} - k_{Ge-Ge}n_2^{Ge-Ge} \quad (12)$$

III. Results and Discussion

A. Quantum Chemistry Calculations. Calculated activation barriers for hydrogen desorption via the prepairing mechanism are shown in Table 1. There is only one direct pathway for hydrogen desorption from the Si−Si and Ge−Ge homodimers. On the other hand, there are two possible pathways for hydrogen desorption from the Ge−Si heterodimer, namely the Ge−Si* and Ge*−Si pathways, where the asterisk denotes the up atom of the transition state. On unconstrained one-dimer clusters, the calculated activation barriers for hydrogen desorption from the Si−Si, Ge*−Si, Ge−Si*, and Ge−Ge dimers show only two distinct values, ∼74 kcal/mol and ∼64 kcal/mol (Table 1). In other words, the calculated desorption barrier depends only on the identity of the up atom of the transition state and not on whether the down atom of the dimer is a Si or Ge atom. Similar effects are observed on three-dimer clusters, whether constraints are applied or not. We also observe cluster size effects on the calculated activation barriers. In particular, the activation barriers on unconstrained Si−Si, Ge−Ge, Ge−Si*, and Ge*−Si three-dimer clusters decrease by 7.9, 9.0, 8.2, and 8.4 kcal/mol, respectively, compared to those calculated on one-dimer clusters (Table 1). On the other hand, we find that imposing constraints on clusters has little effect on the calculated activation barriers for the prepairing mechanism (Table 1).[32]

TABLE 1: Activation Barriers (in kcal/mol) of Hydrogen Desorption from SiGe Alloy Dimers via the Prepairing Mechanism[a]

prepairing mechanism	Si−Si	Ge−Ge	Ge−Si*	Ge*-Si
one-dimer unconstrained	74.1	64.3	74.2	64.0
one-dimer constrained	71.2	61.4	71.9	60.3
three-dimer unconstrained	66.2	53.4[b]	66.0	55.6
three-dimer constrained	64.8	52.4[b]		
zero-point correction	−2.1	−2.4	−2.7	−2.0

[a] The zero-point corrections are calculated from unconstrained one-dimer clusters. The asterisk denotes the up atom of the dimer. [b] Calculated on the $Ge_6Si_{15}H_{20}$ three-dimer cluster.

TABLE 2: Activation Barriers (in kcal/mol) of Hydrogen Desorption from Two Adjacent Si−Si Homodimers via Interdimer Mechanism[a]

adjacent Si−Si dimers	E_A (4H)	E_A (3H)	E_A (2H)
$Si_{15}H_{16}$ unconstrained	59.9	61.8	63.3
$Si_{15}H_{16}$ constrained	59.8	64.8	69.3
$Si_{27}H_{24}$ unconstrained	59.3	60.5	56.0
$Si_{27}H_{24}$ constrained	59.5	62.0	61.2
zero-point correction	−3.9	−2.5	−2.9

[a] The zero-point corrections are calculated from unconstrained two-dimer clusters.

TABLE 3: Activation Barriers (in kcal/mol) of Hydrogen Desorption from Two Adjacent Ge−Ge Homodimers via Interdimer Mechanisms[a]

adjacent Ge−Ge dimers	E_A (4H)	E_A (3H)	E_A (2H)
$Ge_4Si_{11}H_{16}$ unconstrained	46.9	49.8	46.3
$Ge_4Si_{11}H_{16}$ constrained	47.0	52.4	52.6
$Ge_8Si_{19}H_{24}$ unconstrained	45.9	47.0	38.9
$Ge_8Si_{19}H_{24}$ constrained	46.4	48.8	43.6
zero-point correction	−4.0	−1.8	−2.5

[a] The zero point corrections are calculated from unconstrained two-dimer clusters.

We have also determined the activation barriers for hydrogen desorption from adjacent dimers via the 4H, 3H, and 2H interdimer mechanisms and summarize the results in Tables 2 and 3. For the 4H mechanism, we find that the activation barrier does not differ significantly from the energy of desorption. Therefore, there are three distinct activation barriers for hydrogen desorption from SiGe alloy surfaces via the 4H interdimer pathway, namely hydrogen desorption from adjacent Si atoms, adjacent Ge atoms, and adjacent Si and Ge atoms (Tables 2 and 3). For the 3H and 2H mechanisms, the calculated activation barriers follow the order 4H < 3H < 2H. Similar to the prepairing mechanism, we find that the activation barriers for interdimer mechanisms decrease when larger clusters are used. On the other hand, imposing constraints on the clusters decreases the activation barriers for the interdimer mechanisms (Tables 2 and 3).[32]

B. Simulated TPD Spectra on the Si(100)-2×1 and Ge(100)-2×1 Surfaces. To compare the desorption behavior of the prepairing and interdimer mechanisms with experiments, we have simulated the coverage-dependent TPD spectra of hy-

TABLE 4: Kinetic Parameters Used to Simulate TPD of Hydrogen from the Si(100)-2 × 1 and Ge(100)-2 × 1 Surfaces via the Prepairing Mechanism[a]

prepairing mechanism	Si−Si	Ge−Ge
activation barrier (E_A)	62.66	49.99
preexponential factor (ν)	2.40×10^{13}	3.27×10^{13}
π-bond strength (ϵ)	7.41	5.81

[a] The energies are in kcal/mol and zero-point corrected.

TABLE 5: Kinetic Parameters Used to Simulate TPD of Hydrogen from the Si(100)-2 × 1 and Ge(100)-2 × 1 Surfaces via the Interdimer Mechanisms[a]

interdimer mechanism	Si−Si	Ge−Ge
2H barrier (E_{2H})	58.23	41.16
3H barrier (E_{3H})	59.51	47.00
4H barrier (E_{4H})	55.62	42.41
2H pre-factor (ν_{2H})	3.00×10^{12}	3.13×10^{12}
3H pre-factor (ν_{3H})	7.76×10^{12}	1.21×10^{13}
4H pre-factor (ν_{4H})	2.03×10^{13}	1.85×10^{13}
E_{22}	−306.87	−287.08
E_{21}	−227.17	−212.31
E_{adj}	−147.31	−137.42
E_{alt}	−147.44	−137.43
E_{mono}	−153.34	−143.47
E_{10}	−73.69	−68.72
E_{00}	0.00	0.00

[a] The energies are in kcal/mol and are zero point corrected.

drogen desorption from the Si(100)-2 × 1 and the Ge(100)-2 × 1 surfaces. The kinetic parameters and the relative energies of the hydride species for TPD simulations are obtained from DFT calculations. For the prepairing mechanism, the activation barriers are determined using *constrained* $Si_{21}H_{20}$ and $Ge_6Si_{15}H_{20}$ three-dimer clusters, since they give more realistic estimates for the activation barrier. The preexponential factors are estimated from canonical transition state theory using the calculated entropies of activation on one-dimer clusters.[39] Since reaction energies are typically less sensitive to cluster size and constraints, zero-point energies are small compared to the reaction energies. Therefore, the relative energies of the hydride species, as well as the zero-point energies, are obtained from *unconstrained* Si_9H_{12} and $Ge_2Si_7H_{12}$ one-dimer cluster calculations (Table 4). For the interdimer mechanisms, activation barriers from *constrained* $Si_{27}H_{24}$ and $Ge_8Si_{19}H_{24}$ four-dimer clusters are used, and the zero-point energies are determined from calculations on *unconstrained* $Si_{15}H_{16}$ and $Ge_4Si_{11}H_{16}$ two-dimer clusters. The preexponential factors for the 2H and 3H pathways are estimated from canonical transition state theory, similar to the methodology used for the prepairing mechanism. Since we were not able to locate transition states for 4H desorption, the preexponential factors for the 4H pathways are estimated from the Si−H or Ge−H symmetric bending frequencies of the $H_{4-}Si_{15}H_{16}$ and $H_{4-}Ge_4Si_{11}H_{16}$ two-dimer clusters, respectively. The relative energies of the hydride species are obtained from *unconstrained* two-dimer cluster calculations, and the energies are zero-point corrected (Table 5). We choose a linear heating rate of 5 K/s, consistent with the experimental heating rate,[24,29] and a characteristic pumping speed of $\tau = 0.01$, consistent with the range suggested by Yates.[40]

The results of our TPD simulations using the statistical mechanical model are summarized in Figure 3. For the prepairing mechanism, the simulated spectra on Si(100)-2 × 1 and Ge(100)-2 × 1 exhibit peak temperatures of 970 and 770 K, respectively (Figure 3, parts a and b). The peak temperatures remain constant except at low initial hydrogen coverage of 0.1 ML, where the peak temperatures increase by only ∼10 K on both surfaces. The simulated TPD spectra for the prepairing mechanism exhibit near first-order behavior, for which the peak temperatures remain constant at different initial coverages. This aspect of simulated TPD spectra is consistent with experiment

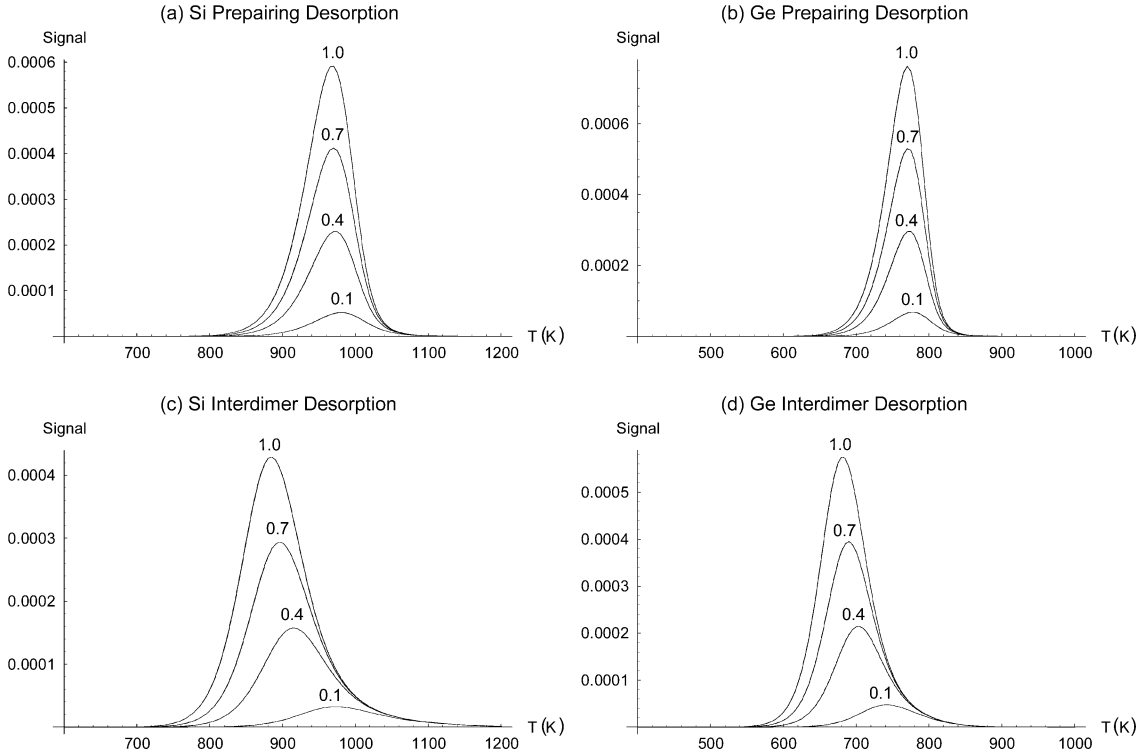

Figure 3. Simulated TPD spectra of hydrogen desorption from the Si(100)-2 × 1 and the Ge(100)-2 × 1 surfaces. Coverage-dependent TPD spectra via the prepairing and interdimer mechanisms are shown. (a) H_2 from the Si(100)-2 × 1 surface via the prepairing mechanism; (b) H_2 from the Ge(100)-2 × 1 surface via the prepairing mechanism; (c) H_2 from the Si(100)-2 × 1 surface via the interdimer mechanisms; (d) H_2 from the Ge(100)-2 × 1 surface via the interdimer mechanisms. The labels on the TPD spectra are the initial hydrogen coverages.

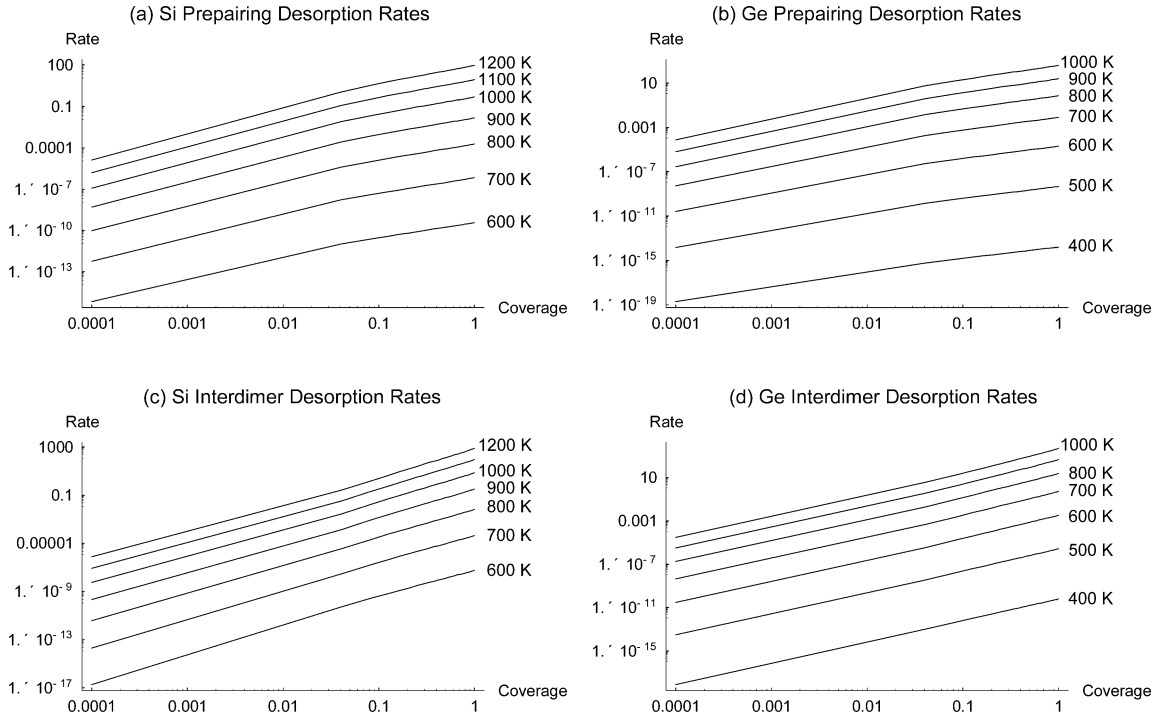

Figure 4. Calculated hydrogen desorption rates on the Si(100)-2 × 1 and the Ge(100)-2 × 1 surfaces. Temperature-dependent desorption rates via the prepairing and interdimer mechanisms are shown. (a) H_2 from the Si(100)-2 × 1 surface via the prepairing mechanism; (b) H_2 from the Ge(100)-2 × 1 surface via the prepairing mechanism; (c) H_2 from the Si(100)-2 × 1 surface via the interdimer mechanisms; (d) H_2 from the Ge(100)-2 × 1 surface via the interdimer mechanisms.

TABLE 6: Apparent Reaction Order of Hydrogen Desorption from the Si(100)-2 × 1 and Ge(100)-2 × 1 Surfaces via the Prepairing and Interdimer Mechanisms at Different Temperatures

T (K)	Si prepairing	Si interdimer	*T* (K)	Ge prepairing	Ge interdimer
600	1.38	2.46	400	1.17	2.03
700	1.47	2.43	500	1.31	2.01
800	1.54	2.39	600	1.42	2.01
900	1.60	2.35	700	1.51	2.01
1000	1.64	2.32	800	1.58	2.01
1100	1.68	2.29	900	1.63	2.01
1200	1.71	2.27	1000	1.67	2.01

on the Si(100)-2 × 1 surface, which also showed constant peak temperature with coverage.[9] In contrast, for hydrogen desorption via the interdimer mechanisms, our simulated TPD spectra show that the peak temperatures decrease with increasing initial coverage (Figures 3c and d). When the initial coverages are 0.1, 0.4, 0.7, and 1.0 ML, the simulations show peak temperatures at 975, 915, 895, and 885 K on the Si(100)-2 × 1 surface, respectively, whereas on the Ge(100)-2 × 1 surface, the corresponding peak temperatures are 740, 700, 690, and 685 K.

Although the prepairing and interdimer mechanisms consist of multiple elementary surface reaction steps, an apparent reaction order for the overall desorption process via each mechanism can be determined when the total desorption rates are plotted versus coverage. Figure 4 shows the total rates of hydrogen desorption predicted using kinetic parameters calculated by DFT at different temperatures, and apparent reaction orders obtained by linear regression of the log−log plots are shown in Table 6. We find that hydrogen desorption from the Si(100)-2 × 1 and Ge(100)-2 × 1 surfaces via the prepairing mechanism has an apparent reaction order that ranges from 1.17 to 1.71, and the reaction order increases as temperature increases. On the other hand, the apparent reaction order for hydrogen desorption via the interdimer mechanisms ranges from 2.01 to 2.46 and the order decreases as temperature increases.

C. Comparison to Experiment. Experimental TPD measurements of hydrogen desorption from the Si(100)-2 × 1 and Ge(100)-2 × 1 surfaces both show near-first-order kinetics, with desorption peak temperatures at 790 and 570 K, respectively. The activation barriers of hydrogen desorption from the Si(100)-2 × 1 and Ge(100)-2 × 1 surfaces were derived from TPD to be 57 and 42 kcal/mol, respectively.[9,21,22,41,42] In general, our simulated TPD spectra exhibit higher desorption temperatures than experiment, and we discuss the discrepancies below.

The simulated desorption temperature is very sensitive to the activation barrier. DFT, although efficient, has a typical error range of a few kcal/mol.[43] According to a Redhead analysis, if the activation barrier decreases from 63 to 57 kcal/mol, the desorption peak temperature downshifts by 90 K. Moreover, canonical transition state theory with DFT entropies and cluster models may not have accurately predicted the preexponential factors for hydrogen desorption on semiconductor surfaces. Increasing the preexponential factor increases the desorption rate directly, which in turn decreases the desorption peak temperature. According to simple Redhead analysis with an activation barrier of 64.0 kcal/mol, a 100-fold increase in the preexponential factor, which is not atypical for surface reactions,[44] results in a downshift of the desorption peak temperature by 115 K. Therefore, the accuracy of the kinetic parameters from DFT calculations and the validity of canonical transition state theory for surface reactions can significantly affect the simulated desorption peak temperatures in the TPD spectra and are expected to be major causes of the discrepancy observed between the model and experiments.

If the prepairing and interdimer mechanisms are compared, it is evident that desorption via the interdimer mechanisms results in lower peak temperatures in the simulated TPD spectra, which are closer to experimental values. This is because the desorption barriers for the interdimer mechanisms are generally lower than those of the prepairing mechanism. However, whereas the prepairing mechanism correctly predicts the near-

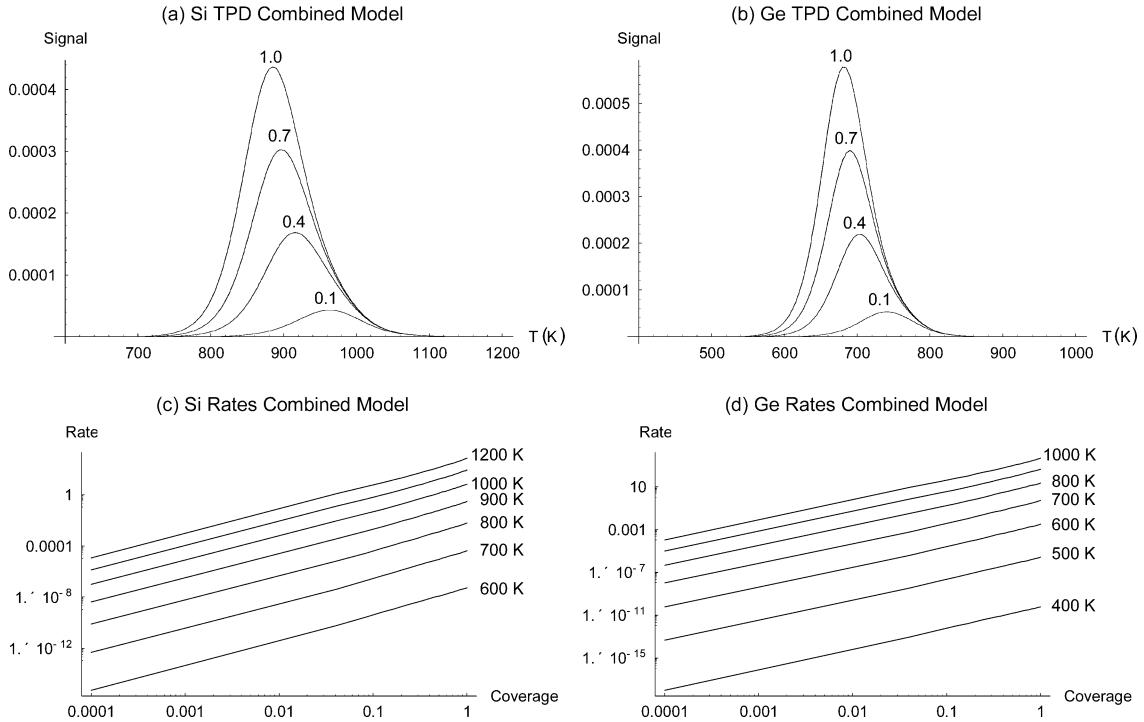

Figure 5. Simulated TPD spectra and calculated desorption rates with the combined model which includes both prepairing and interdimer mechanisms. (a) TPD spectra of H_2 from the Si(100)-2 × 1 surface; (b) TPD spectra of H_2 from the Ge(100)-2 × 1 surface; (c) Desorption rates of H_2 from the Si(100)-2 × 1 surface; (b) Desorption rates of H_2 from the Ge(100)-2 × 1 surface.

first-order desorption behavior of hydrogen on the Si(100)-2 × 1 and Ge(100)-2 × 1 surfaces,[9,18,21,22,41,42] hydrogen desorption via the interdimer mechanisms exhibits reaction orders greater than two on both surfaces, and the desorption peak shifts to lower temperatures with increasing initial coverage. This effect is not in accord with the experimental results, and we discuss the difference between the two mechanisms.

One cause of the differences in the desorption behaviors of the prepairing and interdimer mechanisms is related to the thermodynamic driving force for hydrogen atoms to pair up onto dimers, because it is thermodynamically favorable to have doubly occupied dimers on the surface. Desorption of prepaired hydrogen atoms on the surface results in near-first-order behavior except at low coverages, where the population of doubly occupied dimers decreases and the reaction order increases. For the interdimer mechanisms, there is little or no thermodynamic driving force for the hydrogen atoms to pair up on adjacent dimer sites to form the 2H, 3H, and 4H interdimer structures. As a result, the populations of the interdimer structures are even lower at low hydrogen coverages, which also increases the reaction order of the desorption process.

D. Combination of Prepairing and Interdimer Mechanisms. Our results show that neither the prepairing nor the interdimer mechanisms can completely explain the experimental TPD spectra observed on the Si(100)-2 × 1 and Ge(100)-2 × 1 surfaces. In particular, the prepairing mechanism is consistent with the near-first-order desorption behavior of hydrogen on the two surfaces, whereas the calculated activation barriers for the interdimer mechanisms are closer to the values derived from TPD experiments. Therefore, we attempt to improve our model for hydrogen desorption by including contributions from both the prepairing and interdimer mechanisms. Specifically, prepairing desorption from the n_{mono} species, as well as 2H, 3H, and 4H interdimer desorption from the n_{adj}, n_{21}, and n_{22} species, respectively, are included in the overall rate expression (13). However, although prepairing desorption from the n_{21} and n_{22} hydride species is possible, our calculations indicate the activation barriers of prepairing desorption from these two hydride species, on which the neighboring dimers are occupied with H atoms, are likely to be higher than the activation barrier of 3H and 4H desorption from these two species.[32] In fact, the activation barrier of prepairing desorption from the Si−Si dimer when the neighboring dimers are occupied with hydrogen atoms is 71.4 kcal/mol, whereas 3H and 4H interdimer desorption from hydrogen-occupied neighboring dimers are 60.6 and 59.3 kcal/mol, respectively. Therefore, prepairing desorption from the n_{21} and n_{22} species are not included in the overall rate expression due to their noncompetitive nature. In the combined model, the partition function for hydride species distribution includes seven nondegenerate configurations for hydride species on two adjacent dimers (Figure 2)

$$\frac{d\theta}{dt} = -\frac{k_{4H}}{2}n_{22} - \frac{k_{3H}}{2}n_{21} - \frac{k_{2H}}{2}n_{adj} - \frac{k_{mono}}{2}n_{mono} \quad (13)$$

The TPD spectra and desorption rates simulated using the combined model are shown in Figure 5. We find that the simulated desorption peak temperatures using this combined model are lower than those determined according to the prepairing mechanism but similar to those of the interdimer mechanisms. We also find that the desorption peak temperature determined from the combined model increases with decreasing coverage, similar to the simulated TPD spectra of the interdimer mechanisms. However, the variations of peak temperatures with coverage are smaller than those obtained from the model based solely on the interdimer mechanisms. The simulated TPD spectra (Figure 5, parts a and b) and desorption rates (Figure 5, parts c and d) show that the reaction orders are closer to first-order than that of the interdimer mechanism, although still higher than the desorption order observed experimentally. For example, the apparent reaction order for the combined model of hydrogen

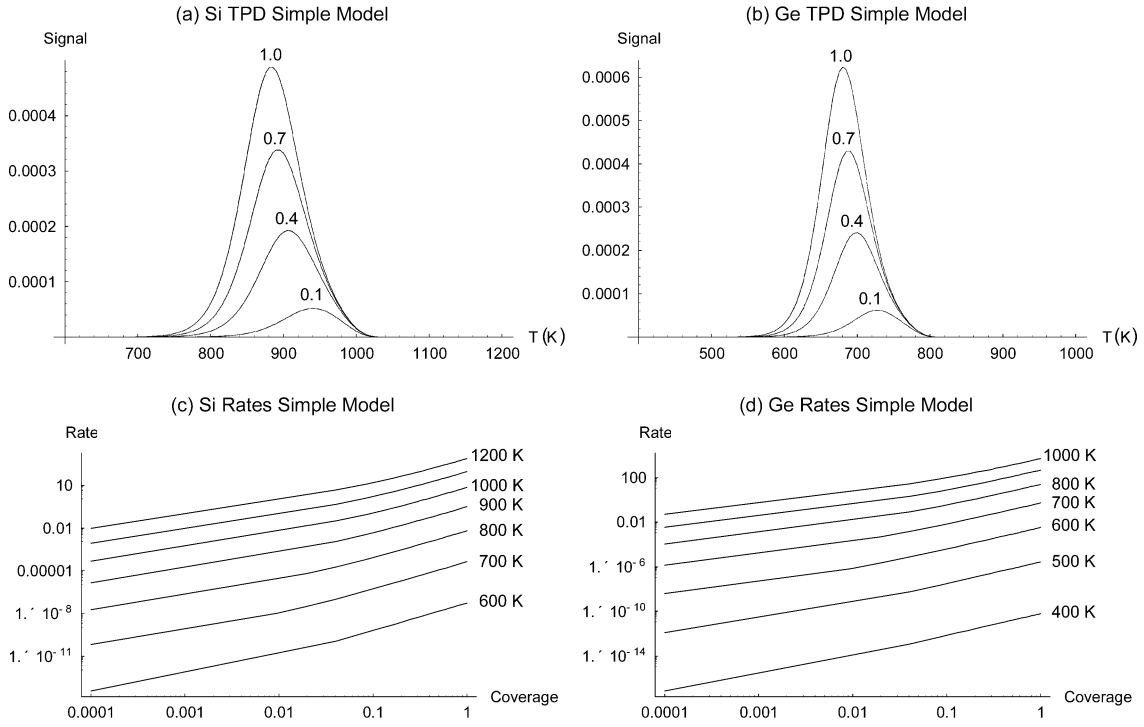

Figure 6. Simulated TPD spectra and calculated desorption rates with the kinetic model based on an alternative hydride distribution partition function. The total hydrogen desorption rate expression includes both prepairing and interdimer mechanisms. (a) TPD spectra of H_2 from the Si(100)-2 × 1 surface; (b) TPD spectra of H_2 from the Ge(100)-2 × 1 surface; (c) Desorption rates of H_2 from the Si(100)-2 × 1 surface; (b) Desorption rates of H_2 from the Ge(100)-2 × 1 surface.

desorption ranges from 1.89 to 2.00 on the Si(100)-2 × 1 surface, and from 1.85 to 2.00 on the Ge(100)-2 × 1 surface.

As the high apparent reaction order observed in the simulated TPD spectra according to the interdimer mechanisms is related to the thermodynamics of the hydride species distribution, the combined model may be improved by considering an alternative hydride distribution. Here, we simulate the TPD spectra of an equilibrium distribution of only the 2H, 4H, and monohydride species (14), as considered by Pan and Zimmermann.[18] Consequently, the total hydrogen desorption rate is comprised of individual desorption rates via the prepairing mechanisms from the monohydride species, as well as the 2H and 4H interdimer mechanisms from the n_{adj} and n_{22} hydride species, respectively (15). The physical justification of the exclusion of the n_{21} configuration is that desorption from the n_{22} species results in the n_{adj} species and that activated migration of hydrogen atoms to the n_{adj} structure is required to form the n_{21} configuration. As a result, if desorption from the n_{adj} configuration is fast relative to formation of the n_{21} structure from the n_{adj} configuration, the exclusion of the 3H pathway is valid. Application of the "fast desorption" assumption also excludes the n_{alt} and n_{10} configurations in the hydride partition functions for interdimer and prepairing desorption, respectively. Activated surface diffusion of hydrogen atoms from the n_{adj} configuration is required to form the n_{alt} species on the surface, whereas prepairing desorption from the n_{mono} species results in the n_{00} species directly

$$Z = \frac{N!2(n_{adj} + n_{mono})}{n_{22}!\,n_{adj}!\,n_{mono}!\,n_{00}!} \exp\left(-\beta \sum_i n_i E_i\right) \qquad (14)$$

$$\frac{d\theta}{dt} = -\frac{k_{4H}}{2} n_{22} - \frac{k_{2H}}{2} n_{adj} - \frac{k_{mono}}{2} n_{mono} \qquad (15)$$

The TPD spectra and desorption rates simulated using the alternative hydride distribution are shown in Figure 6. We find that the peak desorption temperatures determined using the alternative hydride distribution model are similar to those resulting from the combined model. However, variations of peak temperatures with coverage are even smaller than those obtained from the full combined model, and therefore, the reaction orders determined from this alternative hydride distribution kinetic model are closer to first order compared to those obtained from the full combined model. In particular, the apparent reaction order for hydrogen desorption ranges from 1.20 to 1.60 on the Si(100)-2 × 1 surface, while a range of reaction orders between 1.22 and 1.81 is determined on the Ge(100)-2 × 1 surface.

Our kinetic models on hydrogen desorption from the Si(100)-2 × 1 and Ge(100)-2 × 1 surfaces show that the hydride distribution partition function has important effects on the simulated TPD spectra and the overall reaction orders determined from the calculated desorption rates. Inclusion of both the prepairing and interdimer mechanisms in the overall desorption rate expressions within the alternative hydride distribution model results in improvements compared to the kinetic model based on the prepairing mechanism in terms of the simulated desorption peak temperatures. In addition, the overall reaction orders calculated from the combined models are closer to the experimentally observed first order kinetics than the interdimer-based kinetic model. Furthermore, the combined models are more physically realistic because the actual system has both types of desorption pathways available to it simultaneously. However, although the combined models agree better with experiment, they still do not completely capture the experimental observations. Clearly, a combination of accurate kinetic parameters and a good description of the surface chemistry for hydrogen desorption is critical in the modeling and simulation of the desorption process.

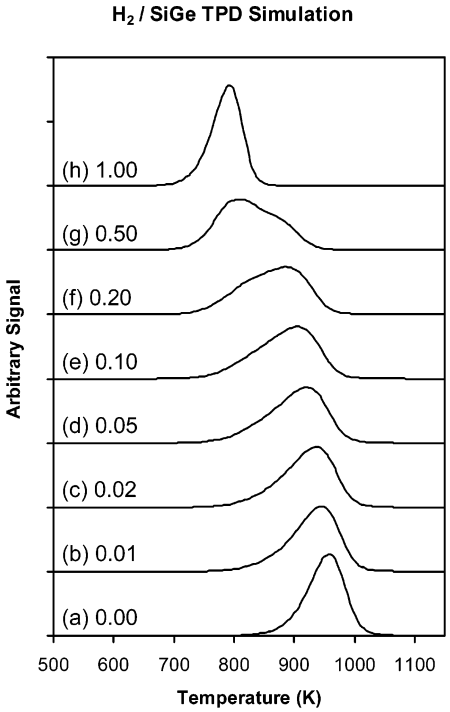

Figure 7. Simulated and experimental TPD spectra of hydrogen desorption from SiGe alloy surface. The initial hydrogen coverages in the simulations are all 1 ML; or one H atom per surface atom. The surface Ge fractions are (a) 0.00; (b) 0.01; (c) 0.02; (d) 0.05; (e) 0.10; (f) 0.20; (g) 0.50; and (h) 1.00.

E. Modeling Hydrogen Desorption from SiGe Alloy Surfaces. In this last section, we discuss hydrogen desorption from SiGe alloy surfaces and address some challenges in modeling the surface chemistry of SiGe alloy surfaces. We will focus on modeling hydrogen desorption via the prepairing mechanism due to its simplicity and its ability to reproduce the near-first-order behavior of hydrogen desorption from the Si(100)-2 × 1 and Ge(100)-2 × 1 surfaces. Our calculations on the prepairing mechanism show that the effect of Ge on hydrogen desorption from SiGe alloy surfaces is local in nature. In other words, the activation barrier for hydrogen desorption via the prepairing mechanism is only affected by the surface dimers onto which hydrogen is adsorbed. An intriguing issue arises from our theoretical predictions: if there are only two distinct activation energies for hydrogen desorption from the SiGe alloy surface, one might first assume that TPD experiments should result in two separate desorption features. Furthermore, the ratio of the peak areas might be expected to be proportional to the ratio of the atomic fractions on the alloy surface, and the desorption temperatures would be expected to be independent of the Ge fraction. However, experimental TPD spectra of hydrogen from SiGe alloy surfaces consist of a single desorption peak up to a surface Ge fraction of 0.1, beyond which a second peak appears. Also, the maximum peak temperature decreases smoothly with surface Ge concentration.[24,26,29] To explain this apparent contradiction, we have simulated the TPD spectra for hydrogen desorption from the SiGe alloy surface. The simulated TPD spectra show that the equilibrium distribution of Si and Ge hydride species can lead to TPD spectra with one Ge-fraction-dependent desorption maximum.

Figure 7 shows the simulated TPD spectra for hydrogen desorption via the prepairing mechanism from SiGe alloy surfaces at full monolayer coverages, using DFT kinetic parameters in Table 7 and the kinetic model discussed earlier. The surface Ge fractions in the simulations are 0.00, 0.01, 0.02, 0.05, 0.10, 0.20, 0.50, and 1.00. The general features of our simulated TPD spectra are consistent with experimental results.[24,26,29] The simulations show that even though there are two distinct activation barriers for hydrogen desorption from different types of SiGe alloy dimers, there is only a single hydrogen desorption peak from SiGe alloy surfaces up to a surface Ge fraction of 0.1, and the desorption peak temperature downshifts as the surface Ge fraction increases. When the Ge fraction is higher than 0.1, a second desorption peak appears, consistent with experiments.[24,26,29]

The desorption behavior of hydrogen on SiGe alloy surfaces can be explained by the distribution of hydride species on the alloy surface. At low Ge surface coverages, hydrogen segregates to surface Si atoms to form Si−H bonds on the surface, because Si−H bonds are stronger than Ge−H bonds. When the surface Ge concentration is increased, thermodynamic equilibrium causes a larger fraction of hydrogen atoms to pair up on Ge-containing dimers, and hydrogen desorption occurs directly from Ge sites. Therefore, the desorption peak temperature downshifts when the surface Ge fraction increases, and a separate peak appears for surface Ge fractions higher than 0.1.

One of the inherent difficulties in modeling SiGe alloy surface chemistry is related to exchange of Ge atoms between the alloy surface and the bulk, because the Ge fraction on the surface can change during a TPD experiment. For example, the TPD studies by Greene and co-workers showed that the desorption temperature depends on both surface as well as bulk Ge concentration of the SiGe alloy.[26] However, our DFT calculations show that bulk Ge atoms do not affect the activation barrier for hydrogen desorption.[32] Given that the effect Ge atoms have on hydrogen desorption from the Si(100)-2 × 1 surface is local in nature, the apparent relationship between the desorption temperature and the bulk Ge composition can be explained not by an electronic influence of bulk Ge atoms on surface hydrogen but rather by segregation of bulk Ge or Si atoms to the surface during TPD. It is known that Ge segregates on the clean Si(100)-2 × 1 surface at high temperatures.[45−49] On the other hand, surface hydrogen can reverse Ge segregation and increase the Si surface composition of SiGe alloy surfaces.[50−53] Although Ge atoms only have a local effect on hydrogen desorption from SiGe alloy surfaces, exchange of surface Si and Ge atoms with

TABLE 7: Kinetic Parameters Used to Simulate TPD of Hydrogen from SiGe Alloy Surface[a]

kinetic parameters and energies	Si−Si	Ge−Ge	Ge*−Si	Si*−Ge
activation barrier (E_A)	64.07	52.89	63.29	53.57
preexponential factor (ν)	2.40×10^{13}	3.27×10^{13}	1.58×10^{13}	1.57×10^{13}
energy of unoccupied dimer	−7.41	−5.81	−6.71	−5.46[b]
energy of singly occupied dimer	−81.12	−73.65	−74.37	−80.53
energy of doubly occupied dimer	−161.10	−147.40	−154.38	−154.38

[a] The asterisk denotes the up atom of the transition states, or the dangling bond in a singly occupied dimer. The energies of the unoccupied, singly occupied and doubly occupied dimers are relative to the energies of the corresponding triplet dimers. The energies are in kcal/mol and zero-point corrected. [b] Although unoccupied Ge−Si* and Ge*−Si dimers have different energies, only the Ge*−Si dimer is considered in the simulations as the ground state of the alloy SiGe heterodimer.

the bulk results in the apparent dependence of hydrogen desorption kinetics on bulk Ge composition of the SiGe alloy.

For hydrogen desorption from SiGe alloy surfaces via the interdimer mechanisms, our simulations show that the effect of surface Ge results in a range of activation barriers for the 2H mechanism, whereas the 4H mechanism has three distinct barriers. Therefore, TPD of hydrogen from SiGe alloy surfaces via interdimer mechanisms should result in Ge-fraction-dependent peak temperatures similar to desorption from SiGe alloy surfaces via the prepairing mechanism. However, modeling the interdimer hydrogen desorption on SiGe alloy surfaces requires the kinetic parameters of all interdimer desorption pathways from adjacent surface dimers with different Ge fractions. For example, there are one, four, six, four, and one possible 2H pathways when there are 0, 1, 2, 3, and 4 Ge atoms on the two adjacent dimers, and consequently, many DFT calculations are required to determine the activation barriers of all of these pathways. Furthermore, these barriers will show a cluster size effect necessitating the need for four-dimer cluster calculations. Therefore, we did not simulate the TPD spectra for hydrogen desorption from SiGe alloy surfaces via the 2H and 4H interdimer mechanisms. Nevertheless, our simulated TPD spectra on SiGe alloy surfaces using the prepairing mechanism show the basic characteristics of the experimental TPD spectra. More importantly, our attempt to model TPD spectra presents a first step toward complete first principles process modeling of SiGe surface chemistry using kinetic parameters predicted by DFT.

IV. Conclusion

In this work, we have used the kinetic parameters determined using DFT to simulate the TPD spectra of hydrogen desorption by the prepairing and interdimer mechanisms. Our results show that, although desorption via interdimer mechanisms results in peak temperatures more consistent with experiments, the temperature-dependent desorption rates show significant deviations from the near-first-order desorption observed experimentally. On the other hand, TPD spectra according to the prepairing mechanism are consistent with the near first-order kinetics observed for hydrogen desorption from the Si(100)-2 $\times$ 1 and Ge(100)-2 $\times$ 1 surfaces, although the peak temperatures are significantly overestimated. We find that the kinetic model including contributions from both the prepairing and interdimer mechanisms agrees better with the experimental TPD spectra. The combined model is also more physically realistic, and its agreement with experiment is further improved by exclusion of the 3H interdimer pathway. Finally, we have simulated the TPD spectra of hydrogen desorption from SiGe alloy surfaces according to the prepairing mechanism, and our simulated TPD spectra are qualitatively consistent with the experimental TPD spectra.

Acknowledgment. C.B.M. gratefully acknowledge the support of the Semiconductor Research Corporation Materials Structures and Devices MARCO Center, the Office of Naval Research, and Stanford's Center for Integrated Systems and Initiative for Nanoscale Materials Processing. S.F.B. acknowledges financial support from the National Science Foundation (CHE 9900041 and 0245260). This work was partially supported by the National Computational Science Alliance (NCSA).

References and Notes

(1) Whall, T. E.; Parker, E. H. C. *Thin Solid Films* **2000**, *367*, 250.
(2) Meyerson, B. S. *IBM J. Res., Dev.* **2000**, *44*, 391.
(3) Presting, H.; Konle, J.; Hepp, M.; Kibbel, H.; Thonke, K.; Sauer, R.; Corbin, E.; Jaros, M. *Opt. Eng.* **2000**, *39*, 2624.
(4) See, P.; Paul, D. J.; Hollander, B.; Mantl, S.; Zozoulenko, I. V.; Berggren, K. F. *IEEE Electron Dev. Lett.* **2001**, *22*, 182.
(5) Paul, D. J. *Adv. Mater.* **1999**, *11*, 191.
(6) Arienzo, M.; Iyer, S. S.; Meyerson, B. S.; Patton, G. L.; Stork, J. M. C. *Appl. Surf. Sci.* **1991**, *48*−*49*, 377.
(7) Greve, D. W. *Mater. Sci. Eng. B* **1993**, *18*, 22.
(8) Joyce, B. A.; Fernandez, J. M.; Xie, M. H.; Matsumura, A.; Zhang, J.; Taylor, A. G. *J. Cryst. Growth* **1996**, *164*, 214.
(9) Sinniah, K.; Sherman, M. G.; Lewis, L. B.; Weinberg, W. H.; Yates, J. T.; Janda, K. C. *J. Chem. Phys.* **1990**, *92*, 5700.
(10) Kolasinski, K. W. *Int. J. Mod. Phys. B* **1995**, *9*, 2753.
(11) Doren, D. J. *Adv. Chem. Phys.* **1996**, *95*, 1.
(12) D'Evelyn, M. P.; Yang, Y. M. L.; Sutcu, L. F. *J. Chem. Phys.* **1992**, *96*, 852.
(13) Hofer, U.; Li, L. P.; Heinz, T. F. *Phys. Rev. B* **1992**, *45*, 9485.
(14) Pal, S.; Doren, D. *J. Chem. Phys.* **1995**, *103*, 1232.
(15) Wu, C. J.; Ionova, I. V.; Carter, E. A. *Surf. Sci.* **1993**, *295*, 64.
(16) Radeke, M. R.; Carter, E. A. *Surf. Sci.* **1996**, *355*, L289.
(17) Biedermann, A.; Knoesel, E.; Hu, Z.; Heinz, T. F. *Phys. Rev. Lett.* **1999**, *83*, 1810.
(18) Zimmermann, F. M.; Pan, X. *Phys. Rev. Lett.* **2000**, *85*, 618.
(19) Durr, M.; Raschke, M. B.; Pehlke, E.; Hofer, U. *Phys. Rev. Lett.* **2001**, *86*, 123.
(20) Buehler, E. J.; Boland, J. J. *Science* **2000**, *290*, 506.
(21) Flowers, M. C.; Jonathan, N. B. H.; Liu, Y.; Morris, A. *J. Chem. Phys.* **1993**, *99*, 7038.
(22) D'Evelyn, M. P.; Cohen, S. M.; Rouchouze, E.; Yang, Y. L. *J. Chem. Phys.* **1993**, *98*, 3560.
(23) Nachtigall, P.; Jordan, K. D.; Sosa, C. *J. Chem. Phys.* **1994**, *101*, 8073.
(24) Ning, B. M. H.; Crowell, J. E. *Surf. Sci.* **1993**, *295*, 79.
(25) Kim, H.; Taylor, N.; Abelson, J. R.; Greene, J. E. *J. Appl. Phys.* **1997**, *82*, 6062.
(26) Kim, H.; Desjardins, P.; Abelson, J. R.; Greene, J. E. *Phys. Rev. B* **1998**, *58*, 4803.
(27) Wu, Y. M.; Baker, J.; Hamilton, P.; Nix, R. M. *Surf. Sci.* **1993**, *295*, 133.
(28) Wu, Y. M.; Nix, R. M. *Surf. Sci.* **1994**, *306*, 59.
(29) Russell, N. M.; Ekerdt, J. G. *Surf. Sci.* **1996**, *369*, 51.
(30) Angot, T.; Louis, P. *Phys. Rev. B* **1999**, *60*, 5938.
(31) Ku, J. H.; Nemanich, R. J. *J. Appl. Phys.* **1996**, *80*, 4715.
(32) Mui, C.; Bent, S. F.; Musgrave, C. B. *J. Phys. Chem. B* **2004**, *108*, 6336.
(33) Hohenberg, P.; Kohn, W. *Phys. Rev.* **1964**, *136*, B864.
(34) Kohn, W.; Sham, L. J. *Phys. Rev.* **1965**, *140*, A1133.
(35) Becke, A. D. *J. Chem. Phys.* **1993**, *98*, 5648.
(36) Frisch, M. J.; Trucks, G. W.; Schlegel, H. B.; Scuseria, G. E.; Robb, M. A.; Cheeseman, J. R.; Zakrzewski, V. G.; Montgomery, J. A. J.; Stratmann, R. E.; Burant, J. C.; Dapprich, S.; Millam, J. M.; Daniels, A. D.; Kudin, K. N.; Strain, M. C.; Farkas, O.; Tomasi, J.; Barone, V.; Cossi, M.; Cammi, R.; Mennucci, B.; Pomelli, C.; Adamo, C.; Clifford, S.; Ochterski, J.; Petersson, G. A.; Ayala, P. Y.; Cui, Q.; Morokuma, K.; Malick, D. K.; Rabuck, A. D.; Raghavachari, K.; Foresman, J. B.; Cioslowski, J.; Ortiz, J. V.; Stefanov, B. B.; Liu, G.; Liashenko, A.; Piskorz, P.; Komaromi, I.; Gomperts, R.; Martin, R. L.; Fox, D. J.; Keith, T.; Al-Laham, M. A.; Peng, C. Y.; Nanayakkara, A.; Gonzalez, C.; Challacombe, M.; Gill, P. M. W.; Johnson, B.; Chen, W.; Wong, M. W.; andres, J. L.; Gonzalez, C.; Head-Gordon, M.; Replogle, E. S.; Pople, J. A. *Gaussian 98*, revision A.5; Gaussian, Inc.: Pittsburgh, PA, 1998.
(37) Russell, N. M.; Ekerdt, J. G. *Surf. Sci.* **1996**, *364*, 199.
(38) Vizoso, J.; Martin, F.; Sune, J.; Nafria, M. *J. Vac. Sci. Technol. A* **1997**, *15*, 2693.
(39) Kolasinski, K. W. *Surface Science: Foundations of Catalysis and Nanoscience*, 1st ed.; John Wiley & Sons Ltd.: New York, 2002.
(40) Yates, J. T. *Experimental Innovations in Surface Science: A Practical Laboratory Methods and Instruments*, 1st ed.; Springer-Verlag: New York, 1998.
(41) Wise, M. L.; Koehler, B. G.; Gupta, P.; Coon, P. A.; George, S. M. *Surf. Sci.* **1991**, *258*, 166.
(42) Lewis, L. B.; Segall, J.; Janda, K. C. *J. Chem. Phys.* **1995**, *102*, 7222.
(43) Petersson, G. A.; Malick, D. K.; Wilson, W. G.; Ochterski, J. W.; Montgomery, J. A.; Frisch, M. J. *J. Chem. Phys.* **1998**, *109*, 10570.
(44) Wang, Z.; Seebauer, E. G. *Appl. Surf. Sci.* **2001**, *181*, 111.
(45) Grutzmacher, D. A.; Sedgwick, T. O.; Powell, A.; Tejwani, M.; Iyer, S. S.; Cotte, J.; Cardone, F. *Appl. Phys. Lett.* **1993**, *63*, 2531.
(46) Godbey, D. J.; Lill, J. V.; Deppe, J.; Hobart, K. D. *Appl. Phys. Lett.* **1994**, *65*, 711.
(47) Godbey, D. J.; Ancona, M. G. *J. Vac. Sci. Technol. A* **1997**, *15*, 976.

(48) Kobayashi, Y.; Sumitomo, K.; Ogino, T. *Surf. Sci.* **1999**, *428*, 229.
(49) Zheng, Y. J.; Lam, A. M.; Engstrom, J. R. *Appl. Phys. Lett.* **1999**, *75*, 817.
(50) Rudkevich, E.; Liu, F.; Savage, D. E.; Kuech, T. F.; McCaughan, L.; Lagally, M. G. *Phys. Rev. Lett.* **1998**, *81*, 3467.
(51) Kobayashi, Y.; Sumitomo, K.; Shiraishi, K.; Urisu, T.; Ogino, T. *Surf. Sci.* **1999**, *436*, 9.
(52) Cakmak, M.; Gay, S. C. A.; Srivastava, G. P. *Surf. Sci.* **2000**, *454*, 166.
(53) Angot, T.; Louis, P. *Phys. Rev. B* **2000**, *61*, 7293.